Journal of Biomedical Optics

BiomedicalOptics.SPIEDigitalLibrary.org

Identification of dirty necrosis in colorectal carcinoma based on multiphoton microscopy

Lianhuang Li
Weizhong Jiang
Yinghong Yang
Zhifen Chen
Changyin Feng
Hongsheng Li
Guoxian Guan
Jianxin Chen

SPIE.

Identification of dirty necrosis in colorectal carcinoma based on multiphoton microscopy

Lianhuang Li,[a,†] Weizhong Jiang,[b,†] Yinghong Yang,[c,†] Zhifen Chen,[b] Changyin Feng,[c] Hongsheng Li,[a] Guoxian Guan,[b,*] and Jianxin Chen[a,*]
[a]Fujian Normal University, Institute of Laser and Optoelectronics Technology, Fujian Provincial Key Laboratory for Photonics Technology, Key Laboratory of OptoElectronic Science and Technology for Medicine of Ministry of Education, Fuzhou 350007, China
[b]Fujian Medical University, The Affiliated Union Hospital, Department of Colorectal Surgery, Fuzhou 350001, China
[c]Fujian Medical University, The Affiliated Union Hospital, Department of Pathology, Fuzhou 350001, China

Abstract. Dirty necrosis within glandular lumina is often considered as a characteristic of colorectal carcinomas (CRCs) that is a diagnostically useful feature of CRCs with DNA microsatellite instability (MSI). Multiphoton microscopy (MPM), which is based on the second-harmonic generation and two-photon excited fluorescence signals, was used to identify dirty necrosis. Our results demonstrated that MPM has the ability to exhibit the microstructure of dirty necrosis and the signal intensity as well as an emission spectrum that can help to differentiate dirty necrosis from cancer cells. These findings indicate that MPM may be helpful in distinguishing MSI colorectal carcinoma via the identification of dirty necrosis.
[DOI: 10.1117/1.JBO.19.6.066008]

Keywords: multiphoton microscopy; colorectal carcinoma; dirty necrosis.

Paper 140116RR received Feb. 26, 2014; revised manuscript received May 21, 2014; accepted for publication Jun. 2, 2014; published online Jun. 26, 2014.

1 Introduction

Dirty necrosis was defined as the presence of cell detritus and inflammatory cells within the glandular lumina. Assessment for the presence or absence of dirty necrosis is often considered as a characteristic of colorectal carcinomas (CRCs). It mainly results from the breakdown of carcinoma cells, which are typically accumulated within the lumina of intact tubular glands, and is more likely related to spontaneous phenomena involving an insufficient vascular supply of the tumor.[1,2] CRCs arise through at least two different molecular genetic pathways in their carcinogenesis: MSI and chromosomal instability.[3] The majority of CRCs arise through chromosomal instability, whereas approximately 15% of tumors arise in the setting of MSI caused by deficiencies in DNA mismatch repair (MMR) machinery. Investigation has shown that lack of dirty necrosis is a diagnostically useful feature of CRCs with DNA MSI.[3] Statistical analysis demonstrated that according to the absence of dirty necrosis, sensitivity and specificity of histologic predictors of MSI status can reach 82.7% and 76.6%, respectively, and when combining the absence of dirty necrosis with tumor infiltrating lymphocytes (TILs) and any mucinous differentiation, the sensitivity can increase to about 100%.[3,4]

As several studies have confirmed that MSI colorectal cancers have a better prognosis than microsatellite stable (MSS) tumors,[5–8] it will become necessary to identify all MSI CRCs so that different therapies are developed to exploit the genetic differences between MSI and MSS tumors. Although dirty necrosis is a simple feature that is readily identifiable by pathologists using routine hematoxylin and eosin (H&E)-stained sections, there are several disadvantages to performing histological biopsies, including sampling error, bleeding, crush artifacts, cost, and time-consuming pathological procedures.[9] Nevertheless, these shortcomings will be surmounted if a multiphoton endoscope is used *in vivo* in the near future.

Multiphoton microscopy (MPM) relies on nonlinear optical processes such as second-harmonic generation (SHG) and two-photon excited fluorescence (TPEF) to achieve high resolution imaging of biological tissues and has been used for tissue imaging. This new imaging technique displays several advantages over these traditional imaging techniques,[10–16] such as real-time, being label-free, near-infrared excitation for superior optical penetration as well as lower photodamage, and it has the ability to detect the cellular and subcellular microstructures of tissues.[17–22] To date, we have no known previous reports that investigated the dirty necrosis in colorectal carcinoma using MPM and this is what motivated us to do this work.

2 Materials and Methods

2.1 *MPM System*

The MPM system has been described previously.[23,24] In brief, a commercial laser scanning microscopic imaging system (LSM 510 META, Zeiss, Jena, Germany) equipped with a mode-locked femtosecond Ti:Sapphire laser (110 fs, 76 MHz) that is tunable from 700 to 980 nm (Coherent Mira 900-F) operating at 810 nm, was utilized to obtain high-resolution images of submucosa in cancerous human rectum tissues. A Plan-Apochromat oil immersion objective (63× and NA = 1.4, Zeiss) was employed for focusing the excitation beam into tissue samples and also for collecting the backscattered intrinsic SHG and TPEF signals. An IR beam block filter (Zeiss KP650), which is in front of the META detector, was used to ensure that the

*Address all correspondence to: Jianxin Chen, E-mail: chenjianxin@fjnu.edu.cn; Guoxian Guan, E-mail: gxguan1108@163.com

†These authors contributed equally to this work.

0091-3286/2014/$25.00 © 2014 SPIE

excitation light was filtered out and only emission signals were recorded. The META detector consists of a high quality reflective grating as a dispersive element and an optimized 32-channel photomultiplier tube array to collect emission signals within the random range from 377 to 716 nm to achieve imaging.

In this work, to simultaneously obtain high-contrast TPEF/SHG images, two independent channels were selected to collect TPEF and SHG signals, respectively. One channel corresponded to the wavelength range of 387 to 419 nm to collect SHG signals (color-coded green), whereas the other channel covered the wavelength range of 430 to 698 nm in order to show TPEF signals (color-coded red). Furthermore, to investigate the spectroscopic characteristics of specimens, the lambda mode was used to carry out spectral imaging and to obtain emission spectra of regions of interest within the spectral image. An optional HRZ 200 fine focusing stage (Carl Zeiss) was used to move the motorized $x-y$ scanning stage for obtaining a large-area image. All images have a 12-bits pixel depth. The images were obtained at 2.56 μs/pixel.

2.2 *Specimen Preparation*

Prior to study participation, all patients signed an informed consent and this study was approved by the Institutional Review Board of the Affiliated Union Hospital, Fujian Medical University. Twelve fresh samples including five colon cancers and seven rectum cancers were obtained immediately after resection from patients for colorectal cancer. The normal tissues were 6 cm away from the cancer margin. Each specimen was sectioned into five serial slices in approximately 10-μm thicknesses. The middle slice was processed for histological examination with H&E stains based on the standard procedures and reviewed by a certified pathologist, then its image was obtained using the standard bright field light microscope (Eclipse Ci-L, Nikon Instruments Inc., Shanghai, Japan) with a CCD (Nikon, DS-Fi2, Japan). The other tissue slices were sandwiched between the microscope slide and a piece of the cover glass for the MPM image.

MPM images showed that five samples, including two colon cancers and three rectum cancers, were scored as having the presence of dirty necrosis which may lead to non-MSI, and then 15 random positions of dirty necrosis were selected. Then, the H&E images from light microscopy (40×) were compared to MPM images for the confirmation of the tissue microstructures revealing that the diagnostic accuracy of MPM was 100%. Finally, the five samples were sent for immunoperoxidase experiments and results demonstrated that these samples did not have MSI. Moreover, to avoid dehydration or shrinkage during the imaging process, a little phosphate-buffered saline solution was dripped onto the specimen.

3 Results and Discussion

Figure 1 shows representative TPEF/SHG images of normal rectal submucosa and the corresponding H&E light microscopic images. Normal rectal submucosa mainly consists of connective tissues including collagen and elastic fibers. Collagens, which have a morphology of fine mesh and are the predominant structural protein in rectum submucosa, are distinctively visualized in Fig. 1(a) via their strong SHG signal, while the elastic fibers, which present a morphology of long-ropes and are much sparser than collagen in rectal submucosa, are displayed very well in Fig. 1(b) by their TPEF signal.[25] Interestingly, in the overlay image of Fig. 1(c), the collagens turn yellowish because they have comparable SHG and TPEF signals.

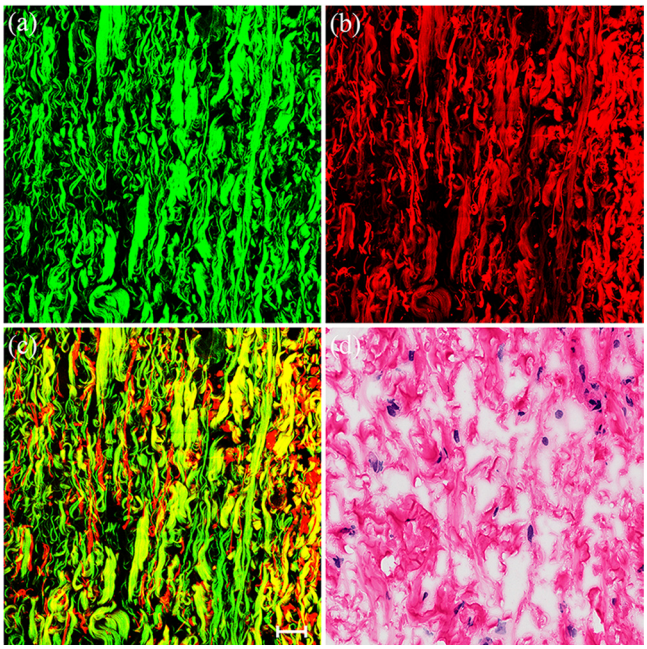

Fig. 1 Representative two-photon excited fluorescence (TPEF)/second-harmonic generation (SHG) images and corresponding hematoxylin and eosin (H&E) image of normal rectal submucosa. (a) SHG image of collagen (color-coded green). (b) TPEF image of collagen and elastic fibers (color-coded red). (c) Overlay of the SHG and TPEF images. (d) The corresponding H&E image (40×). Scale bar: 100 μm.

In comparison to normal tissues, Fig. 2 displays representative SHG/TPEF images of cancerous rectal submucosa and the corresponding H&E image. The collagens as well as elastin fibers obviously display a significant loss compared to normal tissue. The residual collagens become very thin because many abnormal cells infiltrate and displace their locations by degrading collagen, whereas elastic fibers become thick and fragmented (blue arrows). An interest result of blood vessel was found in this layer. The blood vessel wall becomes distorted and uneven (yellow arrow) just because it is compressed by the proliferating cancer cells in cancerous tissue.[26,27]

More importantly, there are many cancerous rectal glands with a disordered arrangement as well as an irregular shape, which are a typical characteristic of adenocarcinoma[28] and indicate that cancerous cells have invaded into the submucosa. Many abnormal cells with circular nuclei and irregular sizes can be clearly discerned in Fig. 2(b). They aggregate in this layer, resulting in high nuclear/cytoplasmic ratios and demonstrating the same morphological characteristics as those of the mucosa.[25,29] The most obvious feature is that there are many fluorophores from dirty necrosis which fill with the irregular glandular lumina (white arrows). This confirms the presence of dirty necrosis. By contrast, the MPM images of glandular lumina are dark because only mucus is in them (pink arrows). Thus, it is very easy to evaluate whether the dirty necrosis is absent or present based on the MPM. These qualitative morphological variations are very consistent with the paired histological sections as shown in Fig. 2(d). To the best of our knowledge,

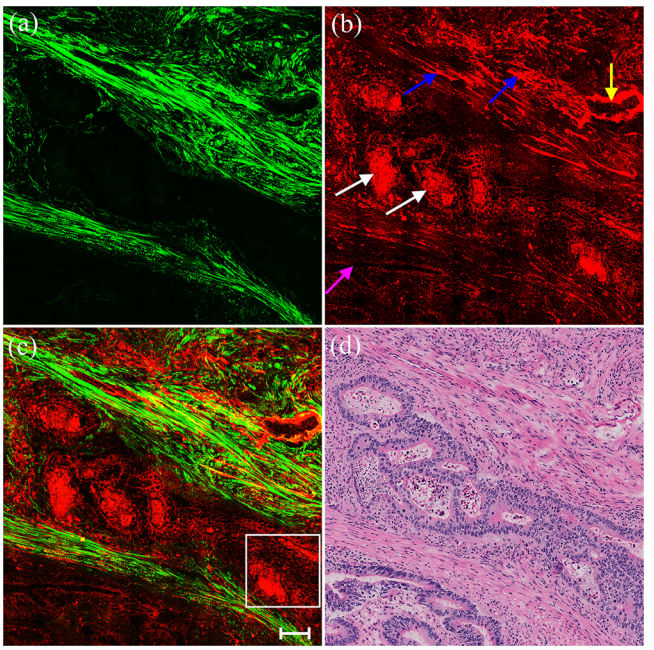

Fig. 2 Representative TPEF/SHG images and corresponding H&E image of cancerous rectal submucosa. (a) SHG image of collagen (color-coded green). (b) TPEF image of dirty necrosis, cancerous cells, blood vessel, collagen, and elastic fibers (color-coded red). (c) Overlay of the SHG and TPEF images. (d) The corresponding H&E image (40×). Scale bar: 100 μm.

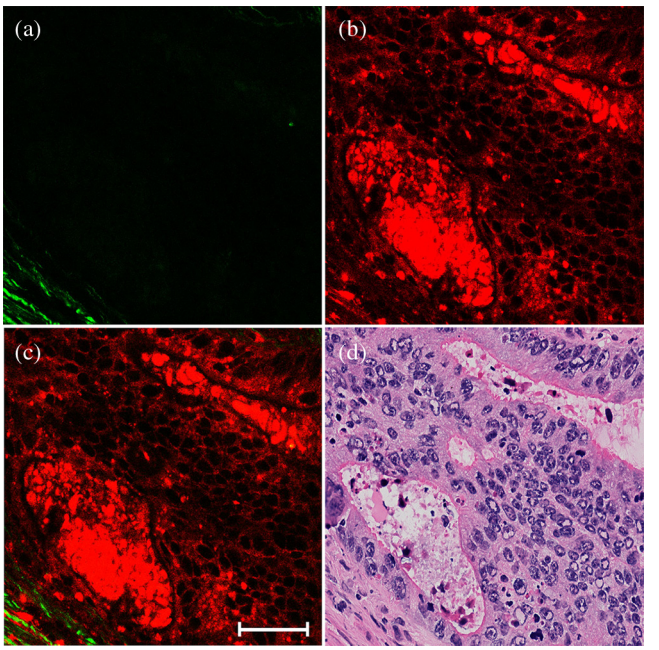

Fig. 3 Magnified image of the region of interest shown in Fig. 2(c) (white box), showing more detailed structural information of dirty necrosis and cancerous cells. (a) SHG image of collagen (color-coded green). (b) TPEF image of carcinomatous cells and dirty necrosis (color-coded red). (c) Overlay of the SHG and TPEF images. (d) The corresponding H&E image. Scale bar: 50 μm.

no other study of MPM imaging about dirty necrosis has been described.

In order to clearly present the microstructures of dirty necrosis and cancerous cells, Fig. 3 shows magnified SHG/TPEF images of the part of the white box in Fig. 2(c) and the corresponding H&E image. It is obvious that the signal intensity from dirty necrosis is far greater than that of cancerous cells. In detail, the mean and standard deviation of emission intensity from dirty necrosis is 1453.60 ± 459.62, while from the cancerous cells is 329.02 ± 141.46, that is, the intensity ratio of dirty necrosis over cancerous cells is approximately 4. Furthermore, to exactly show the characteristic and analyze the constituents of dirty necrosis, emission spectra of dirty necrosis and cancerous cells after subtraction of background were simultaneously obtained under the same conditions by using the image-guide spectral analysis method as shown in Fig. 4, which ensures that they can be compared on same scale. The TPEF signal with three peaks at around 475, 511, and 540 nm was detected. According to the previous study, the fluorescence peaks at 475 and 540 nm were responsible for nicotinamide adenine dinucleotide and flavin adenine dinucleotide, respectively, while the strong fluorescence peak at 511 nm corresponded to a cellular structural protein.[15,23,30]

Dirty necrosis is a constant and diagnostically important histologic feature differentiating types of colon cancers.[4,31,32] In particular, dirty necrosis is negatively associated with MSI and has become an indispensable factor index as one of the pathologic predictors of MSI in colorectal cancer.[2,3,33,34] MSI is the molecular fingerprint of a deficient MMR system and approximately 15% of CRCs arise in the setting of MSI.[35] Several studies have demonstrated that MSI CRCs have a better prognosis than MSS tumors. Hence, identification of MSI colorectal cancers is important, not only for the identification of hereditary nonpolyposis colorectal cancer syndrome but also for tailoring a successful therapy.[36,37]

However, this is an expensive process that requires either DNA testing to identify MSI or immunoperoxidase staining to look for the loss of DNA MMR enzymes.[38–40] Recently, some researchers have described the morphological features of MSI tumors and find that the lack of dirty necrosis is significantly associated with MSI tumors.[3,4,31] This simple characteristic is easily identified from H&E stained histological section, but histological biopsies have several disadvantages including sampling error, bleeding, crush artifacts, and time-consuming pathological procedures.[9] By contrast, MPM imaging of dirty necrosis can provide a real-time noninvasive optical diagnosis for differentiating an MSI colorectal carcinoma that should undergo evaluation to obtain better treatments.

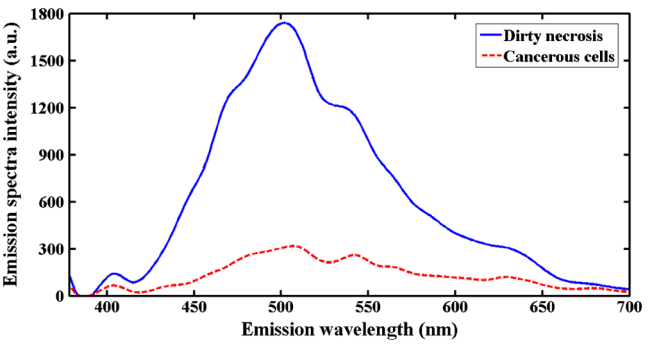

Fig. 4 Emission spectra of dirty necrosis within glandular lumina and cancerous cells from the cancerous rectal submucosa, obtained with an excitation wavelength of 810 nm.

Studies demonstrated that the lack of dirty necrosis was an indispensable factor in predicting MSI status and also an important factor in MMR defects that may cause MSI.[33,34,41] Greenson et al. showed that when it was used alone to predict MSI status, sensitivity and specificity can reach 82.7% and 76.6%, respectively. If combining the absence of dirty necrosis with TILs and any mucinous differentiation, the sensitivity can increase to about 100%.[3] By contrast, if only dirty necrosis can be detected, the tumor may be excluded from MSI tumors. This will be helpful for differentiating MSI tumors from MSS tumors.

Our aim is to introduce a new approach for directly detecting dirty necrosis which may be helpful for MSI testing. MPM may be helpful to prescreen MSI tumors *in vivo* in the future. Although using DNA testing or immunoperoxidase techniques to identify MSI may be more precise for research purposes, it adds additional expense, which we think is not necessary to screen for MSI tumors.

4 Conclusions

In summary, MPM was used to detect dirty necrosis in cancerous rectal submucosa. Our results suggested that MPM can be effective for identifying the dirty necrosis within glandular lumina in rectum cancer, except for differentiating the contents of rectal submucosa including collagen, elastic fibers, and blood vessel. These findings will be helpful for diagnosing MSI colorectal cancer in clinical care. With the continued advancement of miniature multiphoton-based endoscopy, it is foreseen that MPM can benefit *in vivo* diagnosis and treatment in the near future.

Acknowledgments

The work was supported by the Program for Changjiang Scholars and Innovative Research Team in University (Grant No. IRT1115), the National Natural Science Foundation of China (Grant No. 81271620), the Youth Scientific Research Foundation of Fujian Provincial Department of Health (2013-2-36), and National Clinical Key Specialty Construction Project (General Surgery).

References

1. L. Rubbia-Brandt et al., "Importance of histological tumor response assessment in predicting the outcome in patients with colorectal liver metastases treated with neo-adjuvant chemotherapy followed by liver surgery," *Ann. Oncol.* **18**(2), 299–304 (2007).
2. R. H. Lash and W. R. Hart, "Intestinal adenocarcinomas metastatic to the ovaries," *Am. J. Surg. Pathol.* **11**(2), 114–121 (1987).
3. J. K. Greenson et al., "Phenotype of microsatellite unstable colorectal carcinomas: well-differentiated and focally mucinous tumors and the absence of dirty necrosis correlate with microsatellite instability," *Am. J. Surg. Pathol.* **27**(5), 563–570 (2003).
4. B. Halvarsson et al., "Clinicopathologic factors identify sporadic mismatch repair-defective colon cancers," *Am. J. Clin. Pathol.* **129**(2), 238–244 (2008).
5. R. Gryfe et al., "Tumor microsatellite instability and clinical outcome in young patients with colorectal cancer," *N. Engl. J. Med.* **342**(2), 69–77 (2000).
6. W. S. Samowitz et al., "Microsatellite instability in sporadic colon cancer is associated with an improved prognosis at the population level," *Cancer Epidemiol. Biomarkers Prev.* **10**(9), 917–923 (2001).
7. T. Watanabe et al., "Molecular predictors of survival after adjuvant chemotherapy for colon cancer," *N. Engl. J. Med.* **344**(16), 1196–1206 (2001).
8. H. Elsaleh, B. Shannon, and B. Iacopetta, "Microsatellite instability as a molecular marker for very good survival in colorectal cancer patients receiving adjuvant chemotherapy," *Gastroenterology* **120**(5), 1309–1310 (2001).
9. M. G. Ying et al., "Real-time noninvasive optical diagnosis for colorectal cancer using multiphoton microscopy," *Scanning* **34**(3), 181–185 (2012).
10. B. Hamm, R. A. Kubik-Huch, and B. Fleige, "MR imaging and CT of the female pelvis: radiologic-pathologic correlation," *Eur. Radiol.* **9**(1), 3–15 (1999).
11. I. V. Larina et al., "Hemodynamic measurements from individual blood cells in early mammalian embryos with Doppler swept source OCT," *Opt. Lett.* **34**(7), 986–988 (2009).
12. N. Yoshida et al., "Image-enhanced endoscopy for diagnosis of colorectal tumors in view of endoscopic treatment," *World J. Gastrointest. Endosc.* **4**(12), 545–555 (2012).
13. J. C. Jung and M. J. Schnitzer, "Multiphoton endoscopy," *Opt. Lett.* **28**(11), 902–904 (2003).
14. K. Togashi et al., "A comparison of conventional endoscopy, chromoendoscopy, and the optimal-band imaging system for the differentiation of neoplastic and non-neoplastic colonic polyps," *Gastrointest. Endosc.* **69** (3 Part 2), 734–741 (2009).
15. M. Monici, "Cell and tissue autofluorescence research and diagnostic applications," *Biotechnol. Annu. Rev.* **11**, 227–256 (2005).
16. D. Moussata, "The confocal laser endomicroscopy," *Acta Endosc.* **39**(6), 448–451 (2009).
17. E. E. Hoover and J. A. Squier, "Advances in multiphoton microscopy technology," *Nat. Photonics* **7**(2), 93–101 (2013).
18. V. A. Hovhannisyan et al., "Quantifying thermodynamics of collagen thermal denaturation by second harmonic generation imaging," *Appl. Phys. Lett.* **94**(23), 233902 (2009).
19. S. M. Zhuo et al., "Label-free multiphoton imaging and photoablation of preinvasive cancer cells," *Appl. Phys. Lett.* **100**(2), 023703 (2012).
20. M. J. Koehler et al., "In vivo assessment of human skin aging by multiphoton laser scanning tomography," *Opt. Lett.* **31**(19), 2879–2881 (2006).
21. P. J. Campagnola and L. W. Loew, "Second-harmonic imaging microscopy for visualizing biomolecular arrays in cells, tissues and organisms," *Nat. Biotechnol.* **21**(11), 1356–1360 (2003).
22. V. Andresen et al., "Infrared multiphoton microscopy: subcellular-resolved deep tissue imaging," *Curr. Opin. Biotechnol.* **20**(1), 54–62 (2009).
23. J. X. Chen et al., "Depth-resolved spectral imaging of rabbit oesophageal tissue based on two-photon excited fluorescence and second-harmonic generation," *New J. Phys.* **9**(7), 212 (2007).
24. S. M. Zhuo et al., "Multimode nonlinear optical imaging of the dermis in ex vivo human skin based on the combination of multichannel mode and Lambda mode," *Opt. Express* **14**(17), 7810–7820 (2006).
25. N. R. Liu et al., "Multiphoton microscopic imaging of normal human rectum tissue," *Scanning* **32**(6), 347–350 (2010).
26. R. K. Jain, "Molecular regulation of vessel maturation," *Nat. Med.* **9**(6), 685–693 (2003).
27. G. Helmlinger et al., "Solid stress inhibits the growth of multicellular tumor spheroids," *Nat. Biotechnol.* **15**(8), 778–783 (1997).
28. C. S. Fuchs and R. J. Mayer, "Gastric carcinoma," *N. Engl. J. Med.* **333**(1), 32–41 (1995).
29. J. X. Chen et al., "Establishing diagnostic features for identifying the mucosa and submucosa of normal and cancerous gastric tissues by multiphoton microscopy," *Gastrointest. Endosc.* **73**(4), 802–807 (2011).
30. J. C. Kennedy et al., "Clearance times of porphyrin derivatives from mice as measured by in vivo fluorescence spectroscopy," *Photochem. Photobiol.* **39**(6), 729–734 (1984).
31. D. L. Lin et al., "Pulmonary enteric adenocarcinoma with villin brush border immunoreactivity: a case report and literature review," *J. Thorac. Dis.* **5**(1), E17–E20 (2013).
32. M. R. Wick et al., "Sporadic medullary carcinoma of the colon," *Am. J. Clin. Pathol.* **123**(1), 56–65 (2005).
33. J. R. Jass, "Classification of colorectal cancer based on correlation of clinical, morphological and molecular features," *Histopathology* **50**(1), 113–130 (2007).
34. J. K. Greenson et al., "Pathologic predictors of microsatellite instability in colorectal cancer," *Am. J. Surg. Pathol.* **33**(1), 126–133 (2009).
35. E. Vilar and S. B. Gruber, "Microsatellite instability in colorectal cancer—the stable evidence," *Nat. Rev. Clin. Oncol.* **7**(3), 153–162 (2010).

36. J. R. Jass, "HNPCC and sporadic MSI-H colorectal cancer: a review of the morphological similarities and differences," *Fam. Cancer* **3**(2), 93–100 (2004).
37. R. R. Broaddus et al., "Pathologic features of endometrial carcinoma associated with HNPCC," *Cancer* **106**(1), 87–94 (2006).
38. N. M. Lindor et al., "Immunohistochemistry versus microsatellite instability testing in phenotyping colorectal tumors," *J. Clin. Oncol.* **20**(4), 1043–1048 (2002).
39. S. D. Ramsey et al., "Cost-effectiveness of microsatellite instability screening as a method for detecting hereditary nonpolyposis colorectal cancer," *Ann. Intern. Med.* **135**(8 Part 1), 577–588 (2001).
40. A. D. L. Chapelle, "Microsatellite instability phenotype of tumors: genotyping or immunohistochemistry? The jury is still out," *J. Clin. Oncol.* **20**(4), 897–899 (2002).
41. P. Joost et al., "Efficient and reproducible identification of mismatch repair deficient colon cancer-validation of the MMR index and comparison with other predictive models," *BMC Clin. Pathol.* **13**(1), 33 (2013).

Biographies of the authors are not available.